Distribution of Potentially Toxic Elements in the City of Zintan and Its Surroundings (Northwestern Libya) by Surface Soil Sampling

Boris Vakanjac, Zorana Naunović, Vesna Ristić Vakanjac, Tanita Đumić, Saša Bakrač, Jana Štrbački, Vuk Gajić, Taher Mohamed Alzarog

Дигитални репозиторијум Рударско-геолошког факултета Универзитета у Београду

[ДР РГФ]

Distribution of Potentially Toxic Elements in the City of Zintan and Its Surroundings (Northwestern Libya) by Surface Soil Sampling | Boris Vakanjac, Zorana Naunović, Vesna Ristić Vakanjac, Tanita Đumić, Saša Bakrač, Jana Štrbački, Vuk Gajić, Taher Mohamed Alzarog | Minerals | 2023 | |

10.3390/min13081048

http://dr.rgf.bg.ac.rs/s/repo/item/0007740

Article

Distribution of Potentially Toxic Elements in the City of Zintan and Its Surroundings (Northwestern Libya) by Surface Soil Sampling

Boris Vakanjac, Zorana Naunovic, Vesna Ristić Vakanjac, Tanita Đumić, Saša Bakrač, Jana Štrbački, Vuk Gajić and Taher Mohamed Alzarog

Distribution of Potentially Toxic Elements in the City of Zintan and Its Surroundings (Northwestern Libya) by Surface Soil Sampling

Boris Vakanjac [1], Zorana Naunovic [2,*], Vesna Ristić Vakanjac [3,*], Tanita Đumić [4], Saša Bakrač [1], Jana Štrbački [3], Vuk Gajić [5] and Taher Mohamed Alzarog [6]

1   Military Geographical Institute "General Stevan Bošković", 11000 Belgrade, Serbia; boris.vakanjac@vs.rs (B.V.)
2   Faculty of Civil Engineering, University of Belgrade, 11000 Belgrade, Serbia
3   Faculty of Mining and Geology, University of Belgrade, 11000 Belgrade, Serbia
4   Independent Researcher, 11000 Belgrade, Serbia
5   Environment and Sustainable Development, Singidunum University, 11000 Belgrade, Serbia
6   Faculty of Education, University of Al-Zintan, Zintan 501, Libya
*   Correspondence: znaunovic@grf.bg.ac.rs (Z.N.); vesna.ristic@rgf.bg.ac.rs (V.R.V.)

Abstract: The study area is the city of Zintan, in northwestern Libya, which has grown over the past 30 years. Its current population is roughly 30,000. Although the city is in part commercial, most of the population engages in agriculture and primarily grows cereal crops (wheat and barley). The demand of the growing city for agricultural products has increased, intensifying the use of fertilizers, pesticides, and insecticides. Consequently, concentrations of potentially toxic elements (PTE) in the soil have increased. To assess the soil quality (to provide a snapshot of the condition of the soil), systematic sampling was undertaken across a grid of about 2 km × 2 km. The main objective was to determine the chemical and mineral composition of the area of interest, keeping in mind the geological footprint of the terrain. The geologic framework itself is not conducive to elevated concentrations of elements like U, Th, Mo, As, Hg, Pb, and Cr. Therefore, metal concentrations greater than the amounts in the Earth's crust are most likely of anthropogenic origin. A total of 143 samples were collected and chemical analyses were performed using a Thermo Fisher Scientific Niton XL3t GOLDD+ XRF analyzer for the following elements: Mo, Zr, Sr, U, Rb, Th, Pb, Au, Se, As, Hg, Zn, W, Cu, Ni, Co, Fe, Mn, Cr, V, Ti, Sc, Ca, K, S, Ba, Cs, Te, Sb, Sn, Cd, Pd, and Ag. This paper provides examples of elevated concentrations, potentially harmful to the environment, such as those of the following: sulfur of unknown origin (two to three times higher than the Earth's crust average); arsenic, given that there are no related natural phenomena (all the samples measured displayed concentrations higher than those found in the Earth's crust); mercury (concentrations much higher than permissible levels); cesium (additional investigations required to determine the origin); molybdenum; and uranium likely resulting from the use of superphosphates (concentrations nearly always significantly higher than those in the Earth's crust).

Keywords: urban setting; farmland; distribution; potentially toxic elements; Zintan; Libya

1. Introduction

Human activity and the over-exploitation of natural resources degrade the environment, including farmland [1]. Both developed and underdeveloped countries face issues in this regard. The planning of land use is a major challenge [2–5]. It is necessary to meet the demands of the population and, at the same time, keep future generations in mind. This is the goal of urban development, which is quite a task for urban planners and decision makers [6–9]. On the other hand, natural resources are limited, and their quantities will reduce dramatically for future generations [10,11].

Over the past several decades, the global population has grown, and the need for urbanization has increased continuously [12,13]. Potentially toxic elements (PTE) and pollutants are currently major environmental issues [14]. Therefore, they are increasingly the focus of research and studies, particularly in relation to urban land [15,16].

The potentially toxic element (PTE) contamination of soil refers to the excessive deposition of PTEs due to various human activities. In soil mediums, the highest concentrations of PTE and plant toxicity are those of cadmium, lead, zinc, copper, nickel, vanadium, arsenic, etc. [17]. They occur in various forms of impurity, salts, or other compounds (coatings of minerals). They can also be of natural origin from base metals, mineral deposits etc. Usually, on their own, these elements pose no risk to the quality of the environment, but their distribution is highly complex and largely depends on human activity [18,19]. Soil contaminants can accumulate in significant quantities and have numerous ecological consequences [20] not only for the environment, but also for humankind, directly or indirectly. They primarily affect human health directly in situations in which people live on or near degraded land, and if they are under the direct influence of pollutants, or indirectly, if humans use or consume agricultural products grown on poor-quality soil [21–28]. In their review paper [29], Zurqni et al. addressed the applicability of Libyan soil databases, which are necessary for ecosystem services and sustainable-development goals. Recent research in this field has increasingly focused on agriculture and the effects of fertilizers on the quality of soil and, consequently, agricultural products [30–33]. In this regard, this paper analyzes the environmental impact of the urban expansion of the city of Zintan (Libya), based on soil sampling. The objective of this research was to test for pollutants in the Zintan area and describe the distribution of primarily potentially toxic elements (PTE) [17], based on chemical analyses in the laboratory of samples collected in situ.

2. General Characteristics of the Explored Area with Main Geological Settings

2.1. General Characteristics

The research presented in this paper focuses on the Zintan Municipality, in northwestern Libya, 160 km southeast of Tripoli, in the Nafusa Mountains, at elevations ranging from 650 to 710 m. It is situated between the municipalities of Sabratha and Surman to the north, Hammada Al Hammra to the south, Rianah to the northeast, the city of Mezdh to the southeast, and the Rajaban Municipality to the west. On ellipsoid WGS84 in the UTM grid, the area falls within zone 33 N, roughly between e232409 and e242600, and n3531722 and n3541254 (Figure 1).

The city of Zintan has a central core from which roads lead to expanding, randomly constructed settlements, particularly to the south and southeast, which usurp farmland. Zintan is generally surrounded by the Sahara Desert, so it is extremely important to conserve farmland and support life in this city, as well as in other cities of Libya. Of territorial relevance to this research is an area approximately situated along the mountain range in the north to 20 km to the east and up to 10 km to the south.

In its economic history, Zintan has traditionally relied on agriculture. However, it has since become a large commercial center in the Nafusa Mountains, and the majority of its inhabitants engage in trade. Despite the rapid growth of commerce and industry, many inhabitants are still farmers, who grow wheat and barley [34]. Jafara, mountain riverbeds, and Marmoutha have been mostly farmland for a long time. Even though temperatures tend to rise in summer and drop in winter, the climate is relatively temperate throughout the year, and it is conducive to agriculture [34].

Based on the most recent government statistics, the population of Zintan is 30,000. However, the figure is actually much larger when estimates include people from Zintan who reside in other cities [34]. The Nafusa Mountains constitute a boundary between the Libyan coastal lowland to the north, known as Jafara, and a plateau to the south. The sediments of the Tripolitanian plateau dip to the south and north. They constitute most of the Nafusa Mountain plateau, whose elevations in places exceed 750 m [35]. The highland suddenly ends in the north, at an escarpment that creates an elevation difference of up

to 350 m. It extends for some 250 km in Libya, from east of the city of Gharian (~60 km south of Tripoli) to the city of Vazzina on the Tunisian border to the west. Isolated horsts continue into Tunisia, but the region is sparsely populated. There are many deep fluvial valleys which, on their way north (towards Jafara), have incised their beds in this platform.
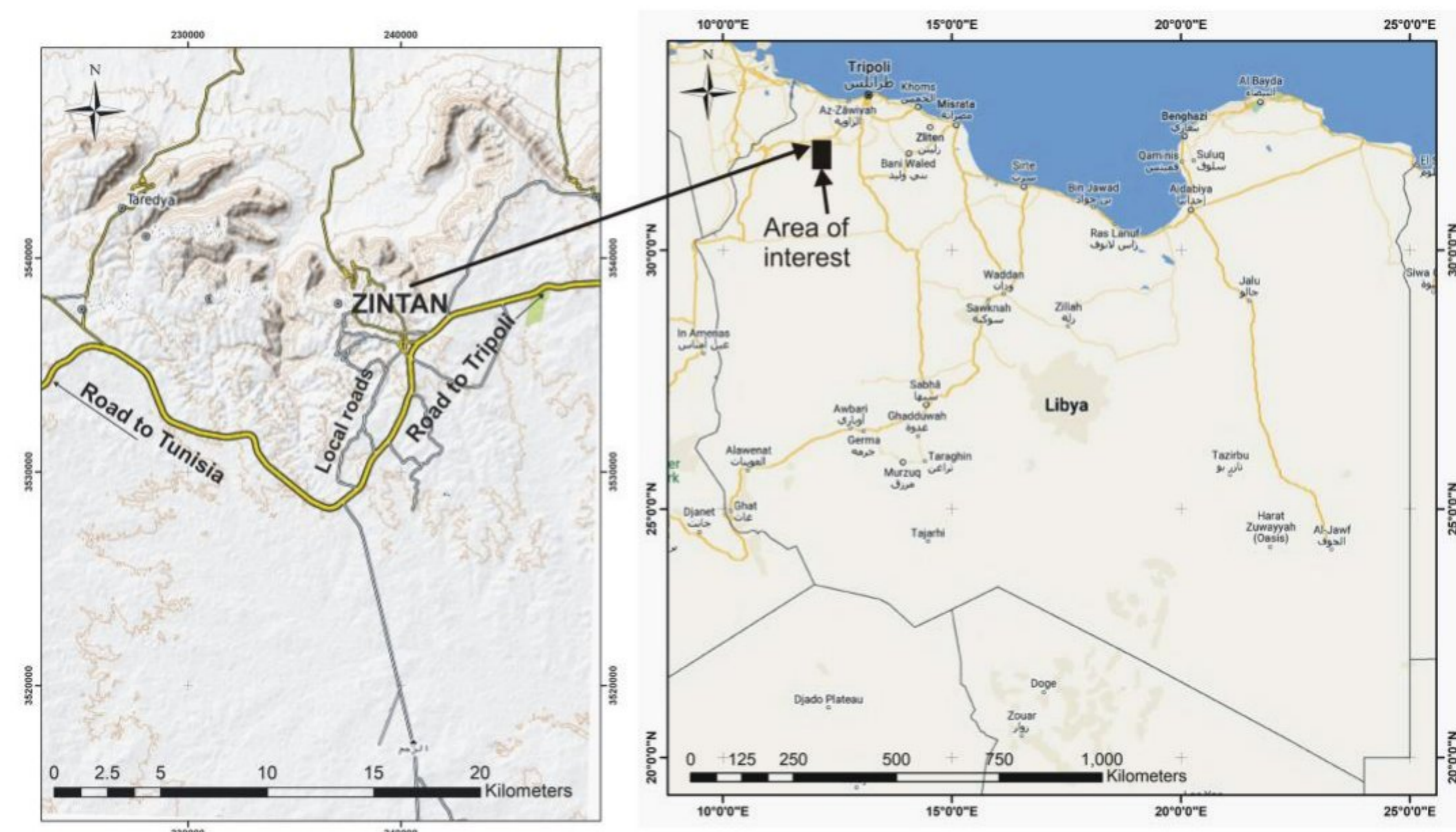
Legend:

	Central part of Zintan		State border
	Settlement		Settlement
	Main road		Area of interest
	Local road		Main roads
	Part of Nafusa mountain		Mediterranean Sea

Figure 1. Geographic position of the study area. **Left**: Raster-based SAS Planet OSM Open Topo Map, and **right**: SAS Planet Map (GoogleMapMaker).

2.2. Main Geological Settings

The geology of the city of Zintan is described in detail on the Libyan state geologic map, Mizdah section NH 33-1, scale 1:250,000 [36]. The geologic units are Upper Cretaceous and Middle Jurassic (Figure 2).

The oldest JmKs Middle Jurassic Kiklah formation, Shakshuk unit is developed in the form of small outcrops and hills that protrude from Quaternary sediments near Zintan and north of Gado. The thickness at the observed sections was around 20 m. Sandy limonitic yellowish-brown limestone was identified, with interbeds of fine gray argillaceous sandstone and mudstone, as well as ferrous gypsum locally. Based on the fossil fauna, the age is Bathonian–Callovian.

The JuKlKr Middle Jurassic/Lower Cretaceous Kiklah formation Al Rajban unit extends along the entire structure, often covered with numerous alluviums. The lower part of this unit is composed of medium-grained yellowish-gray quartz sandstone, with red layers towards the bottom. It is cross-stratified with numerous silicon concretions. The thickness of these sandstones is about 80 m. The underlying member is 40 m thick and composed of conglomeratic sandstones with carbonate cement and gravel up to 2 cm. The unit is overlain by red and white quartz sandstone with clay interbeds.

Figure 2. Geological map of Zintan, Mizdah section [36], modified. The red circle denotes the area of interest.

The KuS Upper Cretaceous unit belongs to the Sidi, as Sid formation of the Cenomanian age. It extends along the Nafusa Mountains. Near Zintan, the rocks are composed of dolomitic limestone, clay, marl, and marly limestone interbeds, overlain by massive

dolomites and limestones from the Nalut formation. The thickness of the Sidi as Sid formation is about 180 m. No identifying fossils were found.

The KuN Upper Cretaceous unit belongs to the Nalut formation from the early Turonian age. It extends along the Nafusa Mountains and is composed of solid and compact carbonate rocks. Their color is light yellowish–gray, and locally red in the upper part. Chert concentrations and nodules are frequent, especially in the upper portions of the sequence. These are recrystallized marly limestones, which are locally dolomitic. is the proportion of $CaCO_3$ is 44% to 62% and that of $MgCO_3$ 35 to 41%. The thickness of the formation is 35 m to 50 m.

The KuT Upper Cretaceous unit belongs to the Quasr Tigrinnah formation of the Turonian–Coniacian age. According to the Mizdah section of the map, it extends as a continuous belt from Gado to Mizdah, with isolated outcrops in the east. The unit is specific because it contains large amounts of gypsum. This gypsum is porous and includes marl, siltstone, clay, and marly limestone interbeds. The interbeds are greenish yellow and 0.5 to 1 m thick. The gypsum deposits are overlain by sequences of marly and chalky limestone.

The KuMm Upper Cretaceous unit belongs to the Mizdah formation, which is divided into Mazuzah and Thala members. The Mazuzah member, from the Santonian age, is in Zintan. Mazuzah is one of the most spacious formations in the Mizdah section. It is composed of limestones, dolomites, and some locally silicified marly limestone. The chemical composition of the limestone is 53% of CaO and 0.7% of MgO. The dolomites contain up to 19% of MgO. The upper sequences of these rocks are 15 to 30 m thick, and largely fine crystalline. In the lower parts, there are marl and chalk interbeds in the limestones, whose thickness ranges from 0.5 to 5 m. Only the lower parts of this formation contain fossils.

3. Methodology

Potentially toxic elements (PTEs) have always been present in the Earth's crust. However, human activity has increased their concentrations [37]. Some of the important influences come from mining, metallurgy, solid-waste disposal, wastewater, and modern agricultural practices that rely on fertilizers, pesticides, insecticides, etc. Because of their toxicity and ability to accumulate in the soil, PTEs are also referred to as environmental pollutants. Pollution by PTEs constitutes a form of abiotic stress, which affects the quality of food as it enters the food chain and is ultimately detrimental to human health [17]. The quantities of ingested PTEs are relatively small, but prolonged intake and the ability of these substances to be stored in the body can lead to various ailments, some of which are ultimately lethal [38]. The impact of PTEs on environmental and human health is very well described in Mitra et al., 2022 [38].

The selected study area, which is the extended area of the city of Zintan, similar to many other urban centers, has grown over the past 30 years. According to the 2012 census, the population was 25,000 [39], but the current population of the city and its environs is estimated at 62,000, probably more [40].

The objective of this research was to test inorganic pollutants (such as Pb, Cr, U, Hg, etc.) in the Zintan area and to describe the distribution of primarily PTEs, based on chemical analyses in the laboratory of samples collected in situ.

The following methods were used.

3.1. Remote Detection

A preliminary study of the area was undertaken using raster-based SAS Planet Map (GoogleMapMaker, version SAS.Planet.Release.160606), SAS Planet Landscape w/o names (Google), and available topographic maps on SAS Planet (Open Street Map—Open Topo Map). This application was then employed to magnify, so that structures could be recognized. Using SAS Planet Bing Maps satellite, the following were identified: (i) densely populated areas; (ii) thinly populated areas; (iii) farmland; (iv) Nafusa Mountains; and (v) lowland with a drainage system northwest of Zintan (Figure 3).
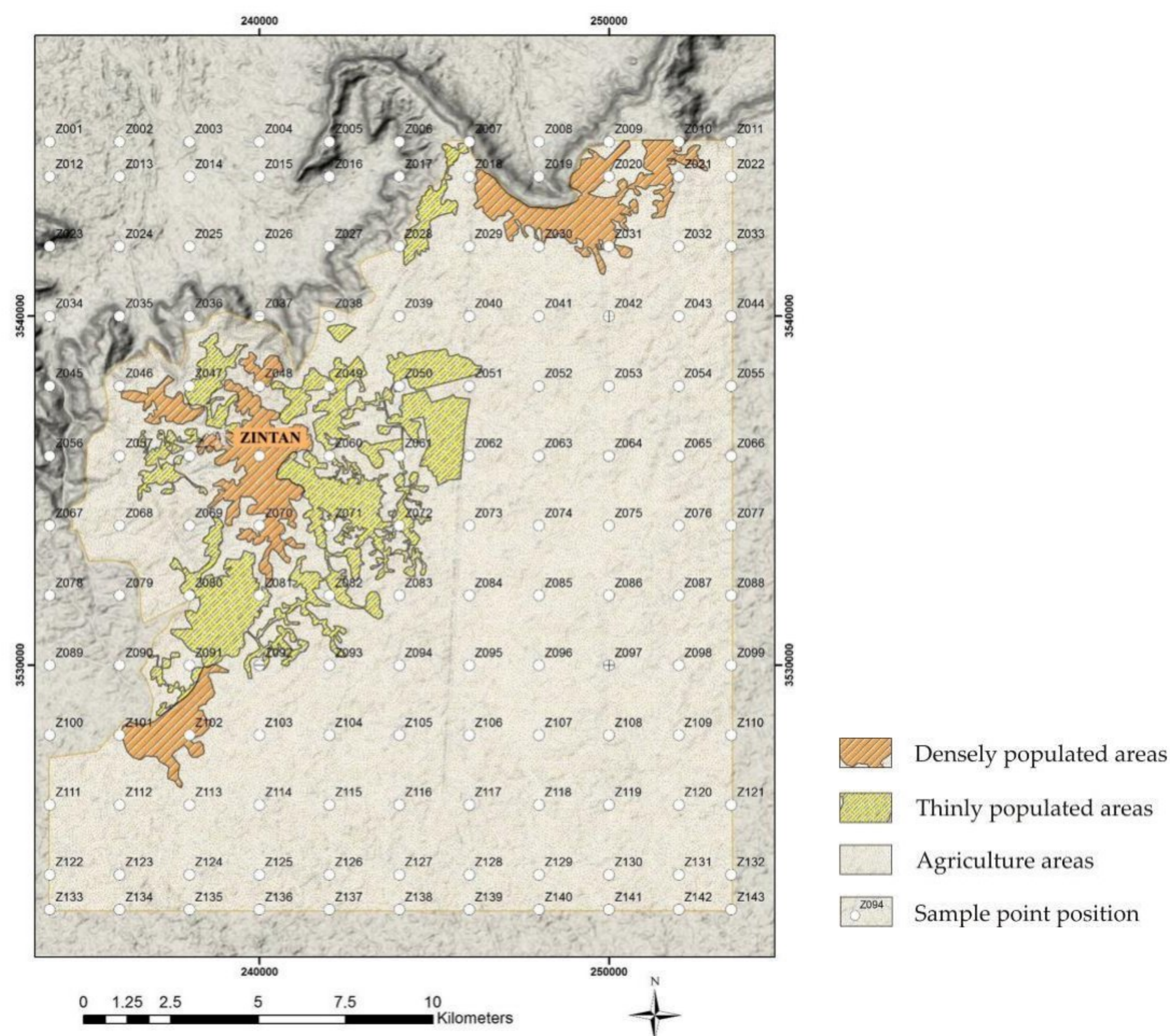
Figure 3. Positions of densely and thinly populated areas, farmland and 143 sampling points, raster-based SAS Planet Landscape w/o names (Google).

3.2. Field Activities—Mapping and Sampling

Samples were collected from predefined locations across an area of 19.5 km × 22 km. The sampling points were spaced 2 km apart, on average (Figure 3). The selection criteria for the sampling points included a generally even distribution and coverage of densely populated areas, sparsely populated areas, and farmland. Information obtained from the Zintan Municipality also needed to be taken into account, concerning the old and recent parts of the city. The GIS base was ellipsoid WGS 84, UTM zone 33. The weights of the samples were from 2 kg to 2.5 kg, and subsequently reduced to 100 g. A total 143 of samples were collected from the surface up to a depth of 250 mm for the purpose of sampling the surface layer of the soil in order to be able to measure elements (and pollutants) at plant-growth level. The samples mainly consisted of cultivated soil with significant sand. In agricultural land, samples were taken between plants. In populated areas, where the terrain was bare and open, it was also quite sandy. The geologic map of Mizdah, scale 1:250,000, indicated that Zintan and its environs are largely situated on Cretaceous sediments overlain by sand. At least two documentary photographs were taken at each observation point.

3.3. Chemical Analyses

Chemical analyses were performed using a Thermo Fisher Scientific (Waltham, MA, USA) Niton XL3t GOLDD+ XRF analyzer at the University of Belgrade Faculty of Civil Engineering. Sample preparation included homogenization, grinding, and sieving. Each sample was then analyzed twice, measured for 240 s in Soil Mode, and checked by the Test All-Geo mode. This testing time was chosen so that limit-of-detection values could be achieved for all the elements. The following elements were measured: Mo, Zr, Sr, U,

Rb, Th, Pb, Au, Se, As, Hg, Zn, W, Cu, Ni, Co, Fe, Mn, Cr, V, Ti, Sc, Ca, K, S, Ba, Cs, Te, Sb, Sn, Cd, Pd, and Ag (33 elements in total). The XRF analyzer was calibrated by performing an auto-calibration system check before the first daily analysis, as well as testing of the verification standards provided by the manufacturer (Thermo Fisher Scientific, Waltham, MA, USA) once a day.

3.4. Modal Analysis of Characteristic Desert-Soil Samples

Light and heavy fractions of ten representative samples were analyzed. Each fraction was observed separately, and microphotographs were taken at the Geological Survey of Serbia. A Karl Zeiss polarizing microscope was used. This was performed on purpose, to determine the mineral compositions of selected samples. Prior to microscopic evaluation, the samples were washed so that the minerals could be recognized. Coating of the minerals by mostly clay and Fe-hydroxides was important, among other aspects, for chemical analyses of the elements of interest. However, it also hindered the determination of the mineral composition. For this reason, the selected samples were washed in order to remove the aforementioned impurities (coatings) and make the minerals easier to recognize.

3.5. Generation of GIS Database

The results were used to create a GIS database that served to determine the distribution of the studied elements.

A GIS program was used for interpolation and spatial distribution. Points of interest with their attributes were generated from the desired Excel file in the database. Next, the Spatial Analyst Tools and the function Spline were used. The Z-value option was used to select the characteristics from the database that we intended to process. The New Spline file appears in the Table of Contents column. A new Layer Properties window opens where Color Ramp can be set. With the Classify option, a new Classification window opens where one of the Classification methods is chosen. Equal Interval was used because it provides good visuals. The result is generated on a map using cell values and the hill-shade effect.

3.6. Multivariate Statistical Analysis

Hierarchical cluster analysis (HCA) is a multivariate statistical method commonly used to group large numbers of samples (e.g., of soil or water), based on similar physical properties and chemical compositions, so that the samples that belong to one cluster have similar characteristics, but they differ from the samples from other clusters [41–44]. The use of HCA supports sample classification based on a large number of variables.

Sample classification based on similarity is referred to as Q-mode cluster analysis, and parameter classification is referred to as R-mode cluster analysis.

The R-mode cluster analysis provided better insights into correlations between the 14 selected parameters, while Q-mode cluster analysis classified the 143 samples into groups with distinctive chemical compositions. Standardized data (*z*-scores) were used in both R-mode and Q-mode HCA. The Euclidian distance (as the measure of similarity) and Ward linkage (as the linkage rule) were applied, since it was determined that they yielded the most diverse clusters.

4. Results

4.1. Modal Analysis of Select Samples

Qualitative and quantitative analyses of the light- and heavy-fraction contents were performed on ten samples, denoted with the letters AZ. The samples were separated into light and heavy minerals using heavy liquids (2.52 g/cm^3). Heavy liquids are usually used in mineral examination to separate "light" minerals, such as quartz, from "heavy" minerals. The density of the liquid used for this type of separation is 2.85 to 2.95 g/cm^3, which is nearly three times the density of water. The heavy liquid used for mineral separation in this case is called LST heavy liquid. This is a concentrated solution of lithium heteropolytungstates in water, which can reach a density of up to 2.95 g/cm^3 at 25 °C and

3.6 g/cm^3 at higher temperatures. It can be diluted with distilled water to a density of 2.52 g/cm^3, which was used in this research [45]. The fractions were immersed in xylol and examined in detail under a Carl Zeiss microscope. The light and heavy fractions were presented as such to explain the mineral compositions of the samples.

Light fraction. The light fraction was generally composed of quartz, rock fragments, clayey and other coated grains, feldspars, calcite, carbonates, and some fossil detritus. The concentration of quartz was the highest of all the samples (Figure 4). The grains were transparent and translucent, semi- to well-rounded, at times with the inclusion of metallic minerals or rutile, zircon, and tourmaline. The surfaces of some of the grains were furrowed and often filled with iron oxides and hydroxides. The feldspars were found to be altered, generally sericitized to a greater or lesser degree. There were only sporadic micas (muscovite and chlorite). The rock fragments were mostly of basite. The coated grains were generally stained with iron oxides and hydroxides [46].

Figure 4. Sample AZ060. (**Left**)—sampling location; (**right**)—microscopic image of sample.

Heavy fraction. The heavy fraction consisted of granate, andalusite, amphiboles, olivine, brookite, distene, leucoxene, rutile, tourmaline, apatite, zircon, biotite, brookite, fossil detritus, and rock fragments. Although present, heavy minerals were rare. Granate was found in three samples, mostly in the form of broken grains with sharp (rarely rounded) edges, light pink in color. Biotite occurred in thin dark-brown plates, and occasionally in dark green, probably chloritized. The tourmaline was identified in shades of gray, in the form of hexagonal prismatic rods. The apatite was colorless and rounded. The zircon was well preserved, partially or fully rounded, colorless or, rarely, light pink. Andalusite was found in irregular, semi-angular grains, with typical pink polychronism. The leucoxene was a secondary mineral in one sample, but only sporadic and ocher-white. The brookite was dark brown, with striations. Amphiboles were detected in three of the samples, in the form of elongated, green, well-rounded grains, at times with iron oxide separations (Figure 5). Rutiles were irregular, rounded, dark red grains. Distene was detected in only one sample, in the form of typical rod-like grains with two distinct splits, colorless or pale blue. The rock fragments were mostly of basite. The coated grains were generally stained with iron oxide and hydroxide. Undeterminable fossil detritus was found in four samples. The mineral association and optical properties of the heavy-fraction minerals indicated aeolian migration and sediment origin. Five samples showed minor input from material from metamorphic rocks [46].

Figure 5. Sample AZ059. (**Left**)—sampling location; (**right**)—microscopic image.

4.2. Spatial Distribution of Investigated Elements

The following reference documents were used in the present study:

(1)   Summary of Maximum Allowable Concentrations of Chemical Constituents In Uncontaminated Soil Used as Fill Material At Regulated Fill Operations (35 Ill. Adm. Code 1100. Subpart F) [47];
(2)   Standards for the contents of PTE metals in soils of some states [48];
(3)   Regulation on the program of systematic soil monitoring, indicators for soil-degradation-risk assessment, and methodology for the development of remediation programs [49];
(4)   Abundance of elements in the Earth's crust [50];
(5)   Terrestrial abundance of elements [51].

Figure 6 is a graphical representation of the concentrations of the analyzed elements in the 143 collected samples. An explanation of the distribution is provided subsequently, from Cr to Zr.
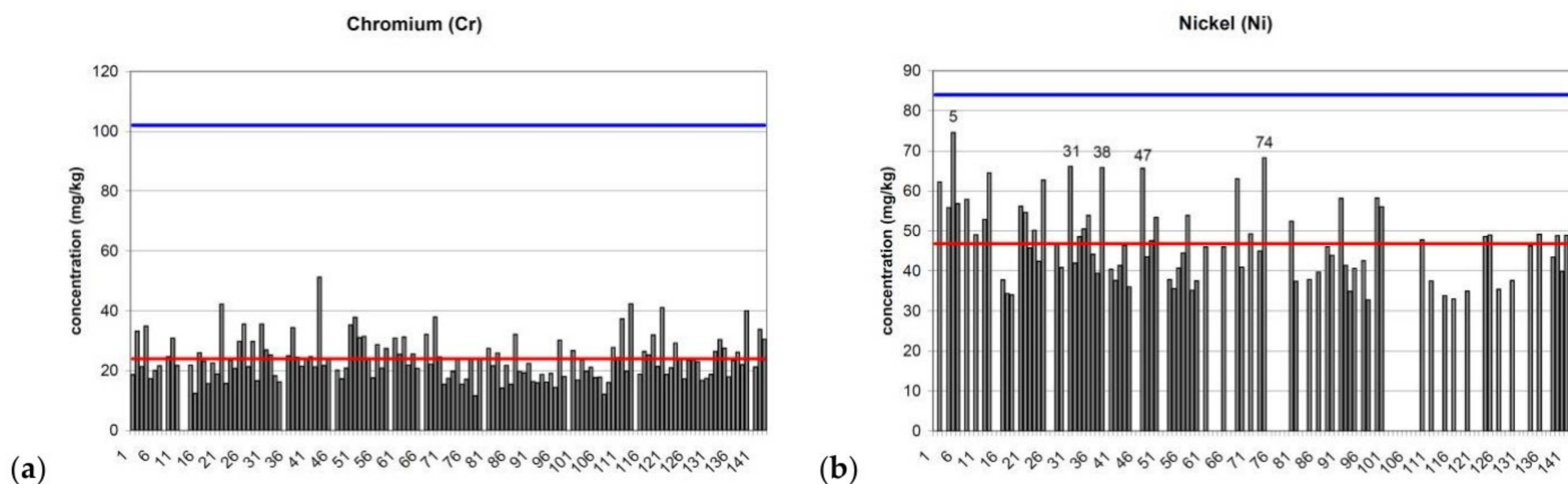
Figure 6. *Cont.*
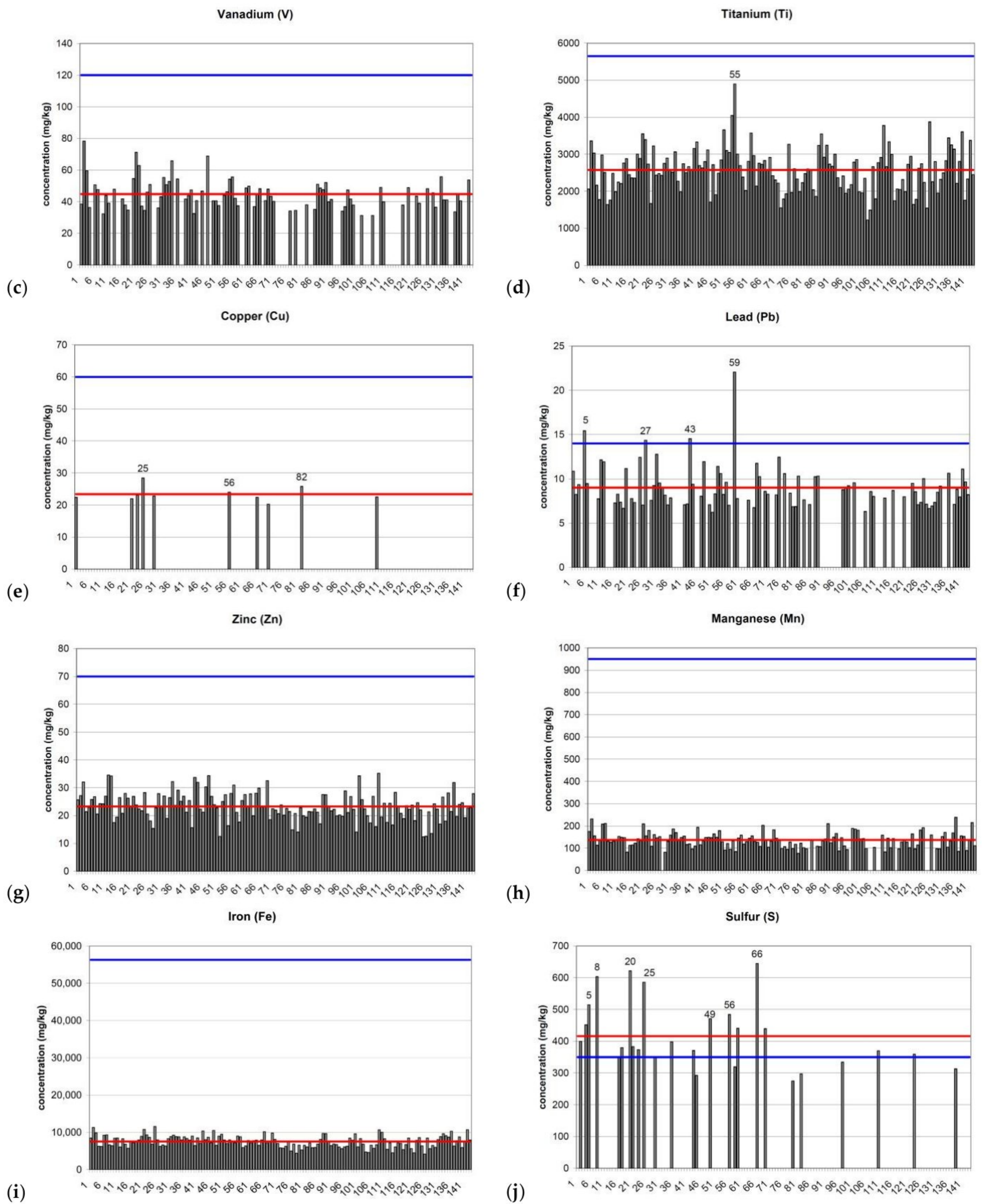
Figure 6. *Cont.*
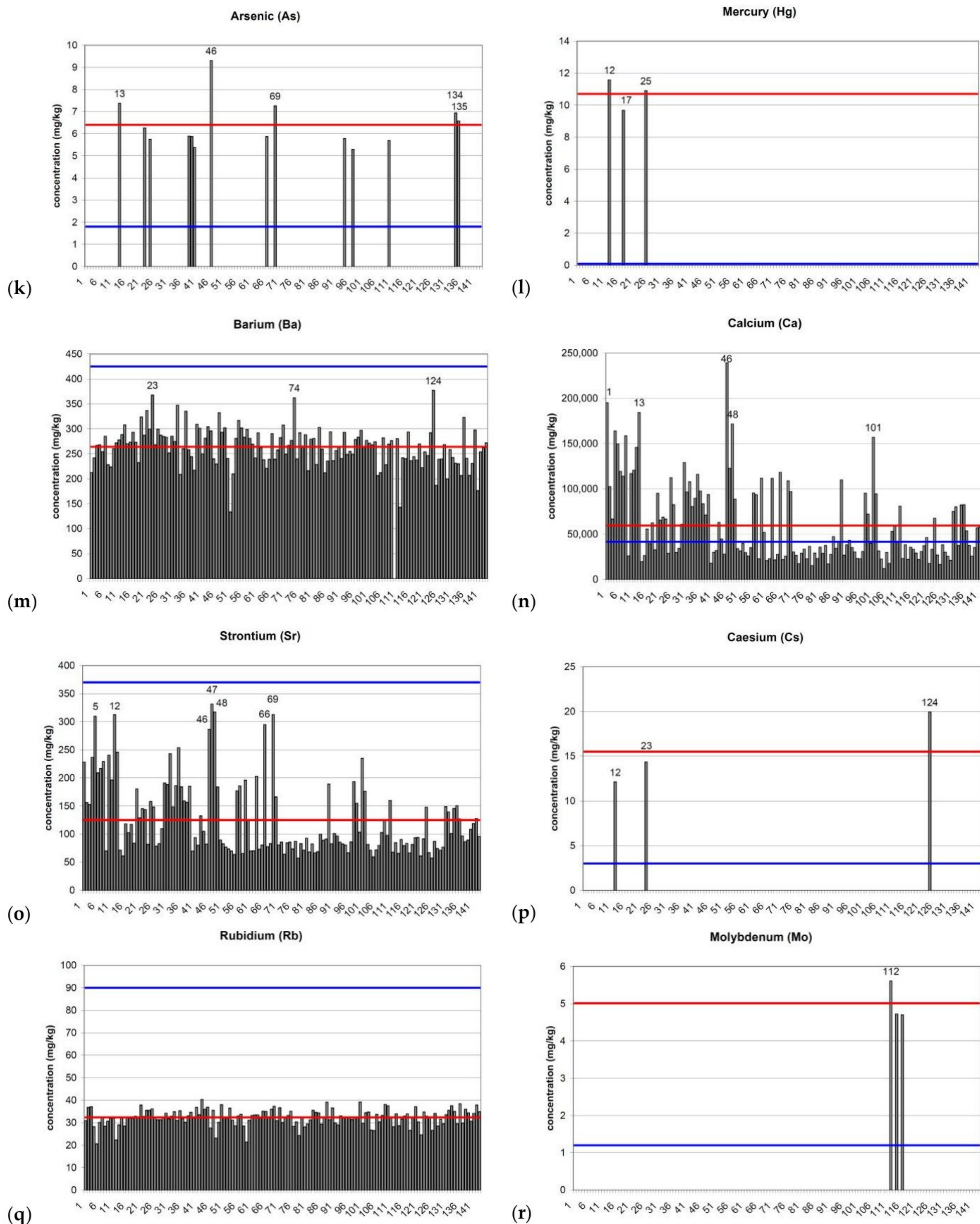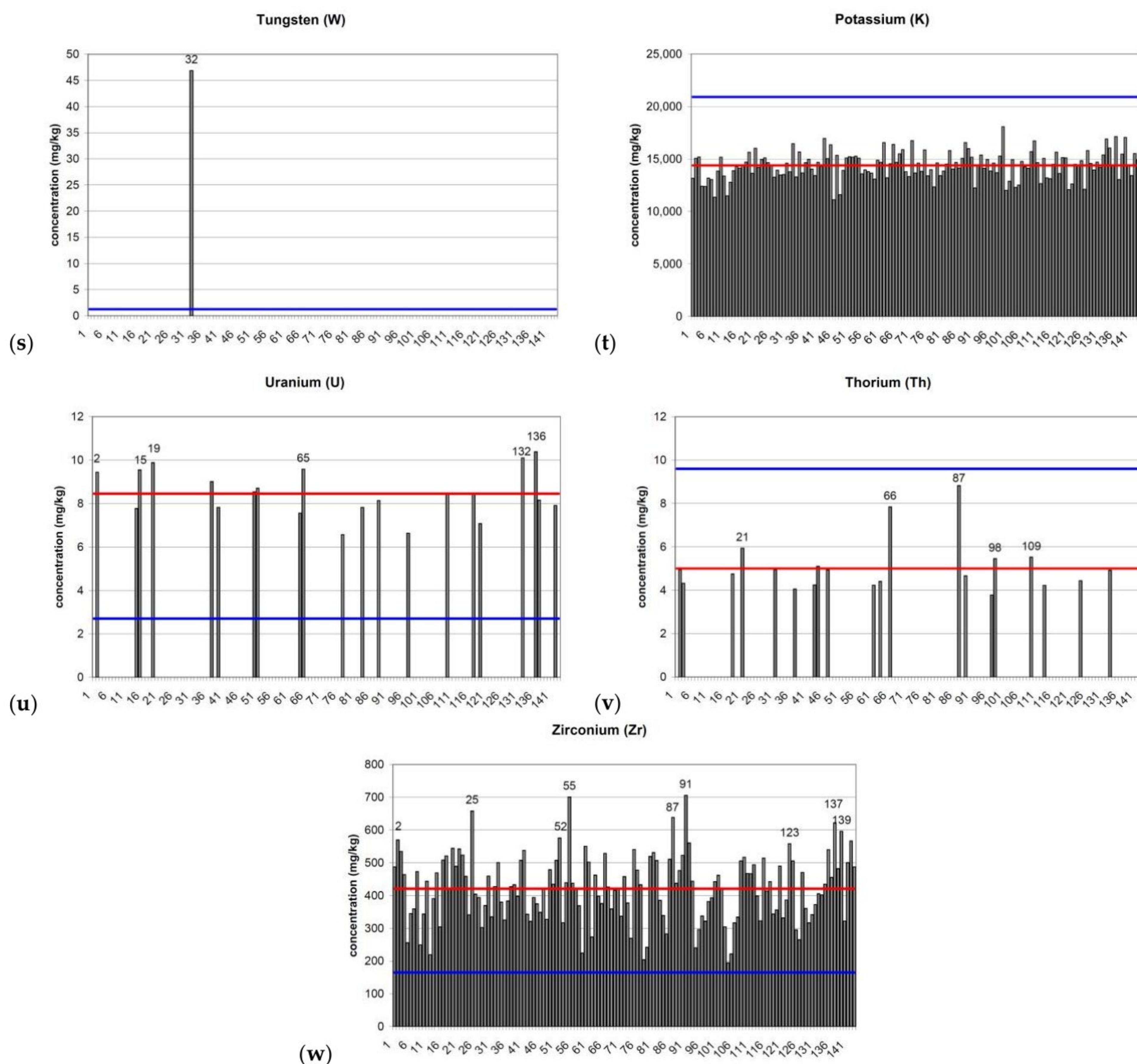
Figure 6. *Cont.*

Figure 6. Concentrations of the studied elements. Legend: blue line—abundance in the Earth's crust, red line—average of particular element (**a**–**w**).

4.3. Multivariate Statistical Analysis

Initial data processing included the detection and the possibility of replacement of missing values. Of the 33 studied elements, 19 were not included in the statistical analysis because of the large number of values below the instrument's limit of detection (>80%). For the remaining 14 elements, the values below the detection limit were replaced with $\frac{1}{2}$ of the detection threshold. The equivocal parameters were Pb, Ni, and V, since 40% of the values were below the limit of detection, which compromised the statistical distribution of the data. However, because of their possible environmental impact, they were not excluded. The concentrations of all the analyzed parameters were expressed in mg/kg.

Elementary statistical quantities were determined for the available set of data, including the minimum, maximum, range, arithmetic and geometric mean, and median (Table 1). Since the concentrations of some of the parameters did not reflect a normal distribution (a lack of correspondence between the arithmetic mean, geomean, and median, i.e., Sr and Ca,

but also Pb, Ni, and V according to the Kolmogorov–Smirnov test of normal distribution), the median values were used instead of the averages (or arithmetic mean).

Table 1. Elementary statistics of the 143 analyzed soil samples (mg/kg).

Parameter	N	Range	Minimum	Maximum	Mean	Standard Deviation	Coefficient of Variation	Median	Geomean
Zr	143	512.0	194.0	706.1	421.3	102.0	0.242	420.5	408.4
Sr	143	274.3	57.12	331.5	125.3	65.48	0.522	93.79	111.9
Rb	143	19.72	20.57	40.29	32.36	3.537	0.109	32.37	32.15
Pb	143	18.06	4.00	22.06	7.09	2.406	0.265	7.12	6.48
Zn	143	22.83	12.36	35.19	23.33	4.885	0.209	22.88	22.80
Ni	143	59.55	15.00	74.55	32.80	9.621	0.206	35.39	28.04
Fe	143	7397	4185	11,582	7537	1549	0.206	7582	7376
Mn	143	213	25.00	238.6	127.7	34.09	0.249	131.6	115.6
Cr	143	40.23	11.00	51.23	22.88	7.051	0.295	21.67	21.67
V	143	65.84	12.50	78.34	31.68	9.132	0.204	36.49	26.39
Ti	143	3673	1224	4897	2575	582.7	0.226	2567	2510
Ca	143	227,218	12,009	239,228	59,443	43,402	0.730	38,142	47,211
K	143	6962	11,104	18,067	14,379	1284	0.089	14,440	14,322
Ba	143	354.5	22.50	377.0	262.4	38.43	0.145	266.8	256.7

The correlations between the parameters were also analyzed. Table 2 shows the correlation coefficients according to Spearman (a non-parametric method suitable where the distribution of data is not normal). High correlation coefficients, greater than 0.5, are highlighted. The correlations between calcium and strontium, potassium and rubidium, and iron and magnesium were pronounced. These were as expected, given their geochemical properties. None of the analyzed parameters indicated a distinct correlation with Pb, Ni, or Ba (the correlation coefficients were around 0.3 or lower).

Table 2. Spearman's coefficients of correlation.

	Zr	Sr	Rb	Pb	Zn	Ni	Fe	Mn	Cr	V	Ti	Ca	K	Ba
Zr	1.00	0.203 *	0.210 *	0.097	0.126	0.062	0.404 **	0.321 **	0.234 **	0.270 **	0.557 **	0.206 *	0.168 *	0.119
Sr	0.203 *	1.00	0.112	0.301 **	0.502 **	0.345 **	0.620 **	0.579 **	0.010	0.307 **	0.043	0.957 **	0.108	0.225 **
Rb	0.210 *	0.112	1.00	0.220 **	0.319 **	0.112	0.643 **	0.351 **	0.390 **	0.372 **	0.456 **	0.062	0.733 **	0.042
Pb	0.097	0.301 **	0.220 **	1.00	0.160	0.222 **	0.364 **	0.313 **	0.091	0.182 *	0.225 **	0.326 **	0.158	0.094
Zn	0.126	0.502 **	0.319 **	0.160	1.00	0.245 **	0.512 **	0.421 **	0.192 *	0.311 **	0.163	0.412 **	0.161	0.268 **
Ni	0.062	0.345 **	0.112	0.222 **	0.245 **	1.00	0.296 **	0.340 **	0.045	0.278 **	0.132	0.316 **	0.054	0.315 **
Fe	0.404 **	0.620 **	0.643 **	0.364 **	0.512 **	0.296 **	1.00	0.691 **	0.385 **	0.660 **	0.588 **	0.600 **	0.475 **	0.207 *
Mn	0.321 **	0.579 **	0.351 **	0.313 **	0.421 **	0.340 **	0.691 **	1.00	0.167 *	0.486 **	0.370 **	0.537 **	0.216 **	0.250 **
Cr	0.234 **	0.010	0.390 **	0.091	0.192 *	0.045	0.385 **	0.167 *	1.00	0.283 **	0.347 **	0.002	0.364 **	0.048
V	0.270 **	0.307 **	0.372 **	0.182 *	0.311 **	0.278 **	0.660 **	0.486 **	0.283 **	1.00	0.520 **	0.287 **	0.276 **	0.192 *
Ti	0.557 **	0.043	0.456 **	0.225 **	0.163	0.132	0.588 **	0.370 **	0.347 **	0.520 **	1.00	0.078	0.548 **	0.106
Ca	0.206 *	0.957 **	0.062	0.326 **	0.412 **	0.316 **	0.600 **	0.537 **	0.002	0.287 **	0.078	1.00	0.132	0.219 **
K	0.168 *	0.108	0.733 **	0.158	0.161	0.054	0.475 **	0.216 **	0.364 **	0.276 **	0.548 **	0.132	1.00	0.079
Ba	0.119	0.225 **	0.042	0.094	0.268 **	0.315 **	0.207 *	0.250 **	0.048	0.192 *	0.106	0.219 **	0.079	1.00

▮	r > 0.7
▮	0.5 < r < 0.7

Significance: *—correlation is significant at the 0.05 level (two-tailed); **—correlation is significant at the 0.01 level (two-tailed).

The results of the R-mode cluster analysis are shown on the dendrogram (Figure 7). There are two distinct clusters. The first is composed of Sr, Ca, Ni, Ba, and Pb. The distance

between the strontium and the calcium is very small, indicating a strong correlation between these parameters (r = 0.957; Table 2). Two subclusters are apparent in the first cluster. The above-mentioned Ca and Sr constitute the first subcluster, and the second is composed of Ni, Ba and Pb, most probably isolated as elements, with no pronounced correlations with any of the analyzed parameters (Table 2).
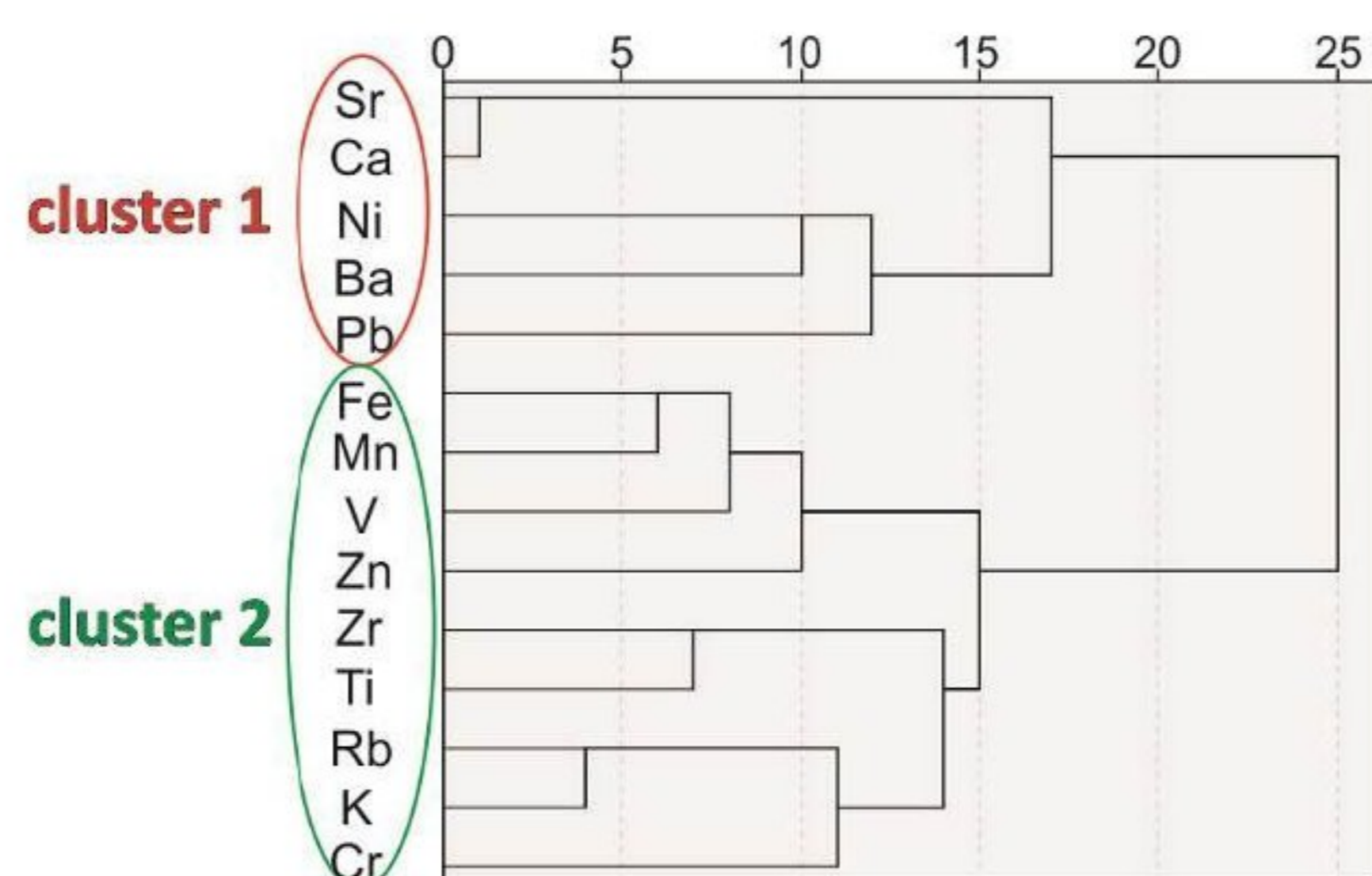
Figure 7. Dendrogram of 14 analyzed elements resulting from R-mode cluster analysis (measure of similarity—Euclidian distance; linkage—Ward method).

The second cluster comprises Fe, Mn, V, Zn, Zr, Ti, Rb, K, and Cr, with small distances between Rb and K (r = 0.733), Fe and Mn (r = 0.691), and Zr and Ti (r = 0.557). The differences between the subclusters are not as pronounced in this case (see Figure 7).

The Q-mode cluster analysis was used to classify the soil samples into three clusters based on a visual inspection of the dendrogram.

The non-parametric Kruskal–Wallis test revealed a statistically significant difference ($p < 0.001$) between the three clusters in terms of the median values of the 14 analyzed variables.

To facilitate the understanding of the chemical properties of the clusters, Table 3 shows the median values of the analyzed variables, used in the Q-mode cluster analysis.

Table 3. Chemical compositions of the clusters—median concentrations of the analyzed elements (mg/kg). Bold values indicate concentrations of individual elements characteristic of a given cluster.

Cluster	1	2	3
No. of samples	35	64	44
Zr	418.8	**469.0**	334.0
Sr	**203.1**	93.05	73.83
Rb	31.86	**34.28**	31.39
Pb	7.85	8.11	4
Zn	25.73	23.70	20.44
Ni	45.71	37.53	15
Fe	8574	7919	6017
Mn	148.4	135.5	97.17
Cr	20.11	**25.45**	18.75
V	41.69	40.87	12.5
Ti	2420	**2905**	2081
Ca	**111,473**	37,781	26,719
K	13,637	**15,092**	13,994
Ba	285.3	262.1	254.4

5. Discussion

The distributions of the detected elements and clusters in the study area are discussed below. On the maps presented in Figures 8–11, the circles of different sizes represent the measured concentration of each element shown on the schematic distribution map. The lower part of each map has a legend showing the concentrations. The maps provide visual information on the distribution of certain elements in the study area, as well as in relation to populated or agricultural areas.
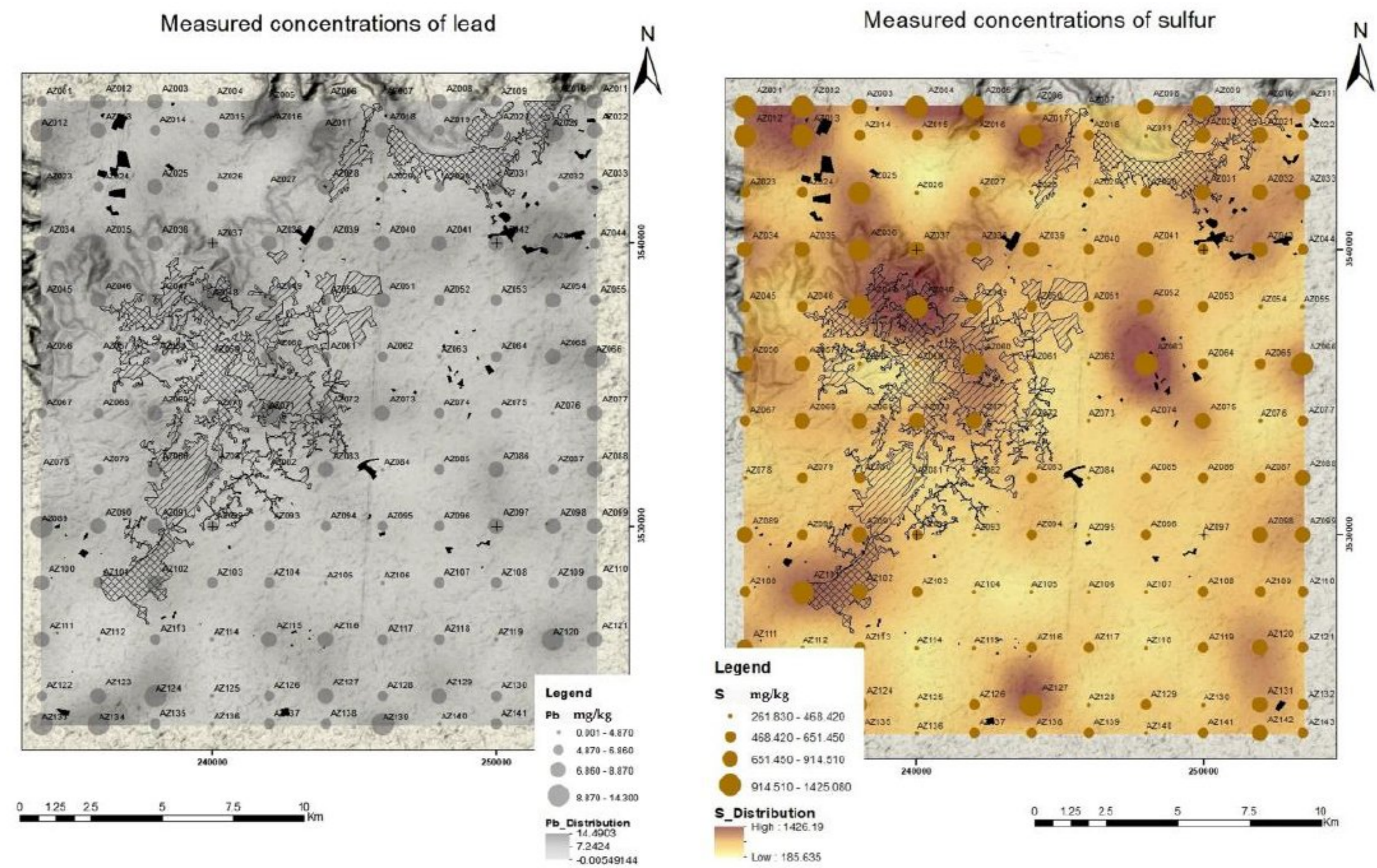
Figure 8. Spatial distribution of lead (**left**) and sulfur (**right**). Raster-based SAS Planet Landscape w/o names (Google).

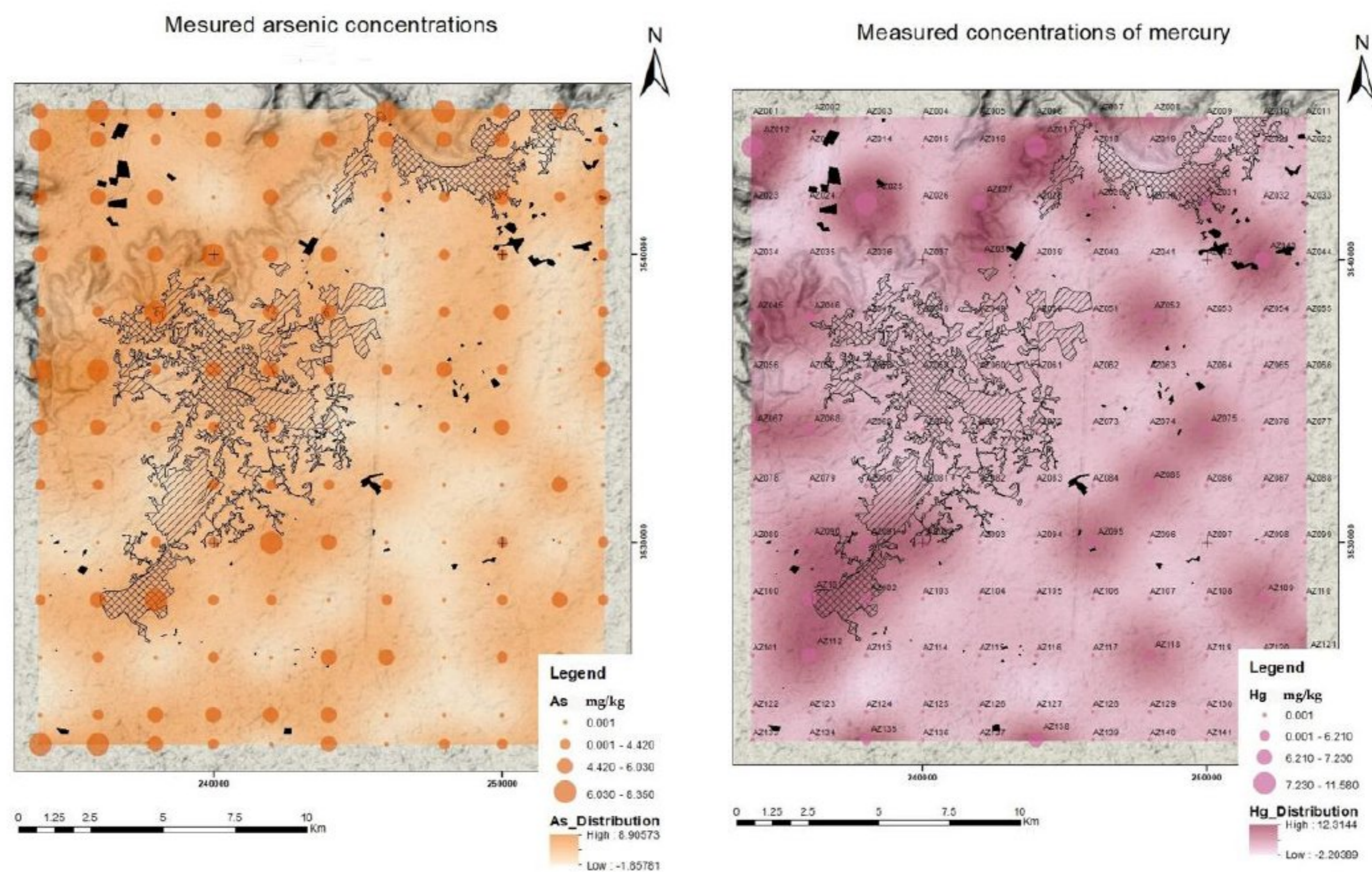**Figure 9.** Spatial distribution of arsenic (**left**) and mercury (**right**), raster based SAS Planet Landscape w/o names (Google).
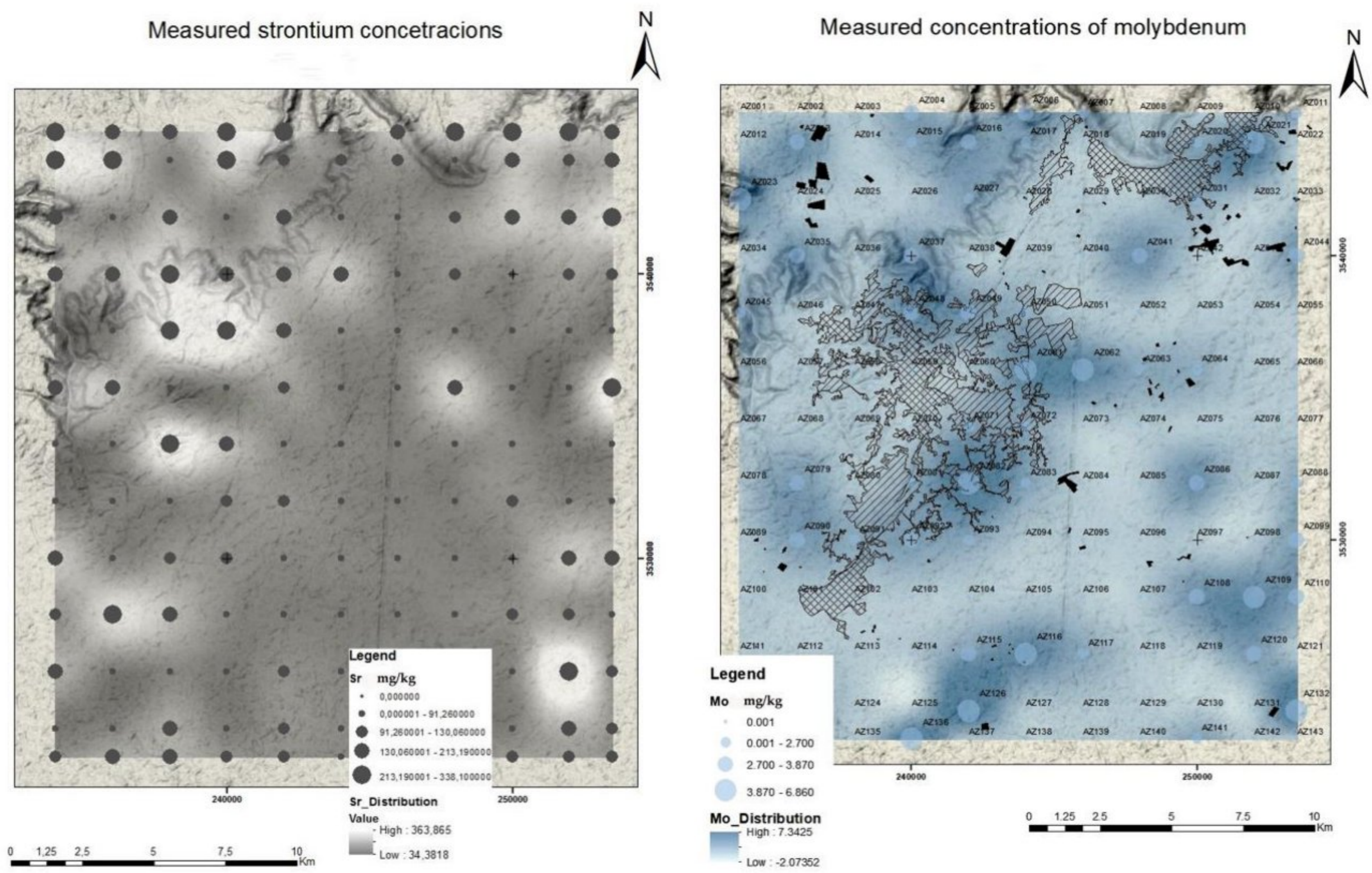
Figure 10. Spatial distribution of strontium (**left**) and molybdenum (**right**). Raster-based SAS Planet Landscape w/o names (Google).
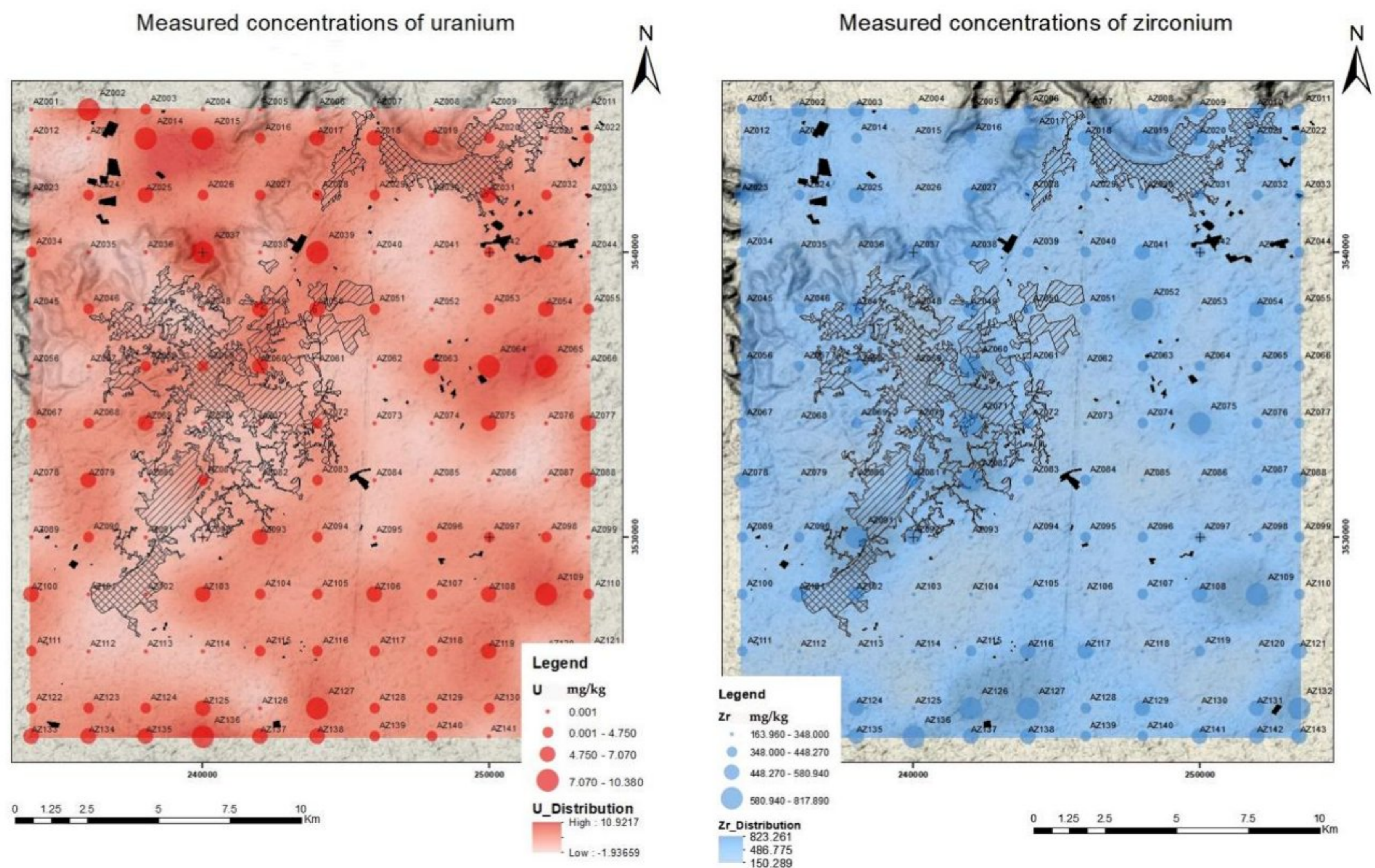

Figure 11. Spatial distribution of uranium (**left**) and zirconium (**right**). Raster-based SAS Planet Landscape w/o names (Google).

5.1. Characteristics of the Distributions of Identified Elements

Chromium and nickel. The highest concentrations were found along the fringes of the densely (rarely thinly) populated areas and in the southeastern/new part of the agricultural area. There were also elevated concentrations of these two elements in the northwestern part of the study area, which is located in the Nafusa Mountains' plateau and horst. The concentrations of some other elements were also elevated. This generally applied to those associated with water-flow directions, which tend to be to the north because the entire area generally dips toward the Mediterranean Sea. In nearly all the samples, Cr was registered, but its concentrations were far below the abundance level, whereas Ni was not detected in 44% of the samples (Figure 6a,b). The Ni concentrations were also below the abundance level. The Cr and Ni concentrations were assumed to be generally natural in origin, with a minor local anthropogenic influence in populated areas.

Vanadium was registered in 84 samples, or 59%. This element generally followed the pattern of the Ni, with its concentrations always below the average in the Earth's crust (Figure 6c). Like the Ni, the V was found in the populated area and on the northwestern plain. It occurred in small amounts in or was entirely missing from the northwestern part, which is composed of recent farmland (according to data from Zintan). Somewhat elevated concentrations were detected in the samples from the eastern fringe of the study area. Given that the rocks there were not V, the origin was assumed to be anthropogenic.

Titanium was found in all the samples (Figure 6d). The lowest concentrations were detected in the new agricultural area, in the direction of the expansion of the city of Zintan. It was also detected on the northwestern plain within the study area. The Ti concentration varied, but based on the map and measured data, it was not certain that the origin was anthropogenic.

Copper was detected in nine samples (Figure 6e). The concentrations were lower than the average in the Earth's crust. However, the occurrence of Cu was not associated with specific areas; it was found in the samples from densely and thinly populated zones, farmland, mountains, and the northwestern plain. Since there were no Cu-bearing rocks, the likely origin is decayed remains of power lines, electric wires, or weapon shells that have begun to oxidize.

Lead exhibited a distribution similar to that of the vanadium. It had no significant presence in the new farmland. The highest concentrations were detected in the populated areas, the northwestern plain, and, at exceptionally high concentrations, in the Nafusa Mountain horsts (Figure 8, Left). Of the 87 samples that registered Pb, the concentrations of only four were above the average in the Earth's crust (Figure 6f). Considering the spatial distribution of Pb, the probable origins are waste dumps with old car batteries, and therefore, presumably anthropogenic.

Zinc was found in all the samples, but in low concentrations—up to half of the average in the Earth's (Figure 6g). Slightly higher concentrations were detected in the populated areas of Zintan, as well as on the northwestern plain. The origins of these elevated concentrations (despite the fact that they were lower than the background levels in the Earth's lithosphere) could be anthropogenic but, in general, they were natural in the majority of the samples.

Manganese was missing or occurred in small quantities in the new farmland. It was widespread in other parts of the study area, but at very low concentrations (3–5 times lower than the average in the Earth's crust) (Figure 6h). Given that elevated concentrations were found in urban as well as mountainous areas, it is safe to assume that the origin is both natural and anthropogenic.

Iron is widespread and found almost everywhere on the planet. It also occurs in the study area, but in very low concentrations. It was detected in all the samples, in uniform concentrations (Figure 6i). The sand was always yellowish-brown due to iron oxides and hydroxides. The highest Fe concentrations were lower than the average in the Earth's crust by a factor of five to six. Slightly higher concentrations were found in the samples collected from the thinly populated parts of Zintan.

Sulfur was mainly detected in the north–northwestern and eastern parts of the study area, and always in populated zones, the mountains, and on the northwestern plain (Figure 8 Right). The concentrations were borderline or slightly higher than in the Earth's crust (Figure 6j). It appeared that elevated concentrations were associated with local occurrences of gypsum, but they were not sufficiently high to be a human health risk. The three points in the city itself, along an almost straight line, were probably associated with facilities that use S. The S was found in 26 samples, of which 21 were borderline and five were above the maximum permissible concentration (MPC). However, none of the concentrations was more than three times higher than the Earth's crust average. Additional investigations are required to determine whether the origin is natural (e.g., gypsum) or anthropogenic (tire dumps or remnants).

Arsenic was found in only 14 samples. The concentrations were always higher than MPC (4.5 mg/kg), by a factor of up to two (Figure 6k). The highest concentrations were detected within the city, and somewhat lower were found at several points in the eastern parts of the study area, as well as, on two locations, in the new agricultural area (Figure 9, Left). This arsenic was probably of anthropogenic origin and transported with leached water along the drainage systems (two locations on the northwestern plain). In all the samples, the As concentration was always above MPC [52]. The geologic framework of the study area does not include any rocks that contain As. The origin of As is most probably pesticides [53].

Mercury was detected in only three samples, in concentrations higher than MPC by a factor of 5–6 (Figure 6l). None of the samples were associated with anthropogenic sources or human activity, based on the available data. However, beyond the urban area, the origin was most probably anthropogenic. Two points were on the northwestern plain and one on the slopes of the Nafusa Mountains (Figure 9, Right). The sampling locations of Hg need to be investigated because their origin is possibly anthropogenic, related to pesticides.

Barium was detected in all the samples (Figure 6m). The concentrations were "naturally" non-uniform. Regardless of the area, the concentrations varied from three times lower than to nearly equal to the lower standard values of the Earth's crust (340–380–500 mg/kg). The origin is natural.

Calcium was determined microscopically in the carbonate samples. The highest concentrations were up to five times greater than background levels and were measured in the samples collected from the Nafusa Mountains (Figure 6n). In this case, the origin of the Ca was natural. It migrated from the mountains to lower elevations.

Strontium had the same distribution pattern as Ca, so the two were clearly correlated (correlation coefficient 0.93; closely positioned on the R-mode dendrogram). Sr was detected in all the samples, but always below the background levels of the Earth's crust (Figure 6o). The origin was natural (Figure 10 Left).

Based on the results, the Ca and Sr concentrations exhibited the best correlations (r = 0.957, Table 2). They were recorded in all the samples, and their highest concentrations were related to the Nafusa Mountains. There is migration of these elements from the mountains to lower elevations, they have similar chemical patterns, and they easily replace each other in the natural environment [54]. They were present in the samples as a result of natural geological settings.

Cesium was found in three samples collected from the northwestern part of the study area. All the concentrations were above MPC, by a factor as high as six (Figure 6p). Of the three samples, two came from a location near the area where the Hg was detected. It should be noted that the origin of the elevated concentrations of Hg and Cs should be investigated further. Like in the case of Hg, one sample of Cs was collected on a slope of the Nafusa Mountains towards the northwestern plain, but on the western side, and the other two came from the plain. It is questionable whether these three locations have an environmental impact. This element is generally used in the drilling of fluid for the oil industry and was most probably of anthropogenic origin [55].

Rubidium, like Ca and Sr, was found in all the samples, in relatively uniform concentrations (Figure 6q). The origin was natural and the concentrations much lower than the abundance level in the Earth's crust.

The elements Rb, K, Sr, Ba, Fe, Mn, V, Ti, Cr, and Ni were found in all the samples, with concentrations lower than those in the Earth's crust. They originate in olivine basalts and meta basalt cones, as well as outcrop varieties of the same rocks from the Pleistocene age, which are located 45 to 95 km west of Zintan [36,56,57]. The concentrations of individual elements were strongly correlated. For example: Rb and K (r = 0.733), Rb and Fe (r = 0.643), Fe and V (r = 0.660), Fe and Ti (r = 0.588), etc. (see Table 2).

Molybdenum was detected in the samples collected 2 km north of the southern boundary of the study area, from agricultural soil (Figure 10 Right). The origin is probably anthropogenic. It is present is Clusters 1 and 2. All the concentrations were above the permissible 3 mg/kg (5.61, 4.72 and 4.7 mg/kg) (Figure 6r). The concentrations were not much higher than MPC [52]. The Mo probably originated in pesticides because it is often used as an agent that improves nitrogen fixation and enhances the absorption of other nutrients from the soil [58].

Tungsten was detected in only one sample. The concentration did not exceed the background levels. Therefore, this finding is of no particular relevance (Figure 6s).

Potassium was found in all the samples. Like in the case of the Ca, Sr, and Rb, the concentrations were relatively uniform (maximum-to-minimum ratio 2:1) (Figure 6t). These concentrations did not exceed the background levels of the Earth's crust. The origin is natural.

Uranium was detected in 21 samples. All but two were collected in unpopulated areas (three on the northwestern plain, one on a slope of the Nafusa Mountains, and the remaining fifteen in farmland). The values were anomalous (Figure 6u). The samples collected from the farmland and the two from the fringes of a sparsely populated area probably registered U due to the use of superphosphates, suggesting that their origins were anthropogenic (Figure 11 Left). This is mainly related to the 12 samples in Cluster 2, which values of concentrations were several times higher than MPC. None of the rocks in the area are natural carriers of U. Nevertheless, the sampling points with grades from, for instance, 8.15 mg/kg to 10.38 mg/kg, should be investigated further.

Thorium was found in 20 samples, and its concentrations did not exceed the background levels in the Earth's crust (Figure 6v). It was largely detected in samples from the eastern agricultural area, as well as in three samples collected along the fringe of a densely populated part of Zintan. The distributions of the U and Th were conditionally associated, indicating that their origins were natural. However, Th can also occur in superphosphates.

Zirconium was detected in all the samples (Figure 6w) and most probably occurred in a mineral identified as zircon, which is rather stable in atmospheric conditions and often a constituent of desert sand. The concentrations of Zr in the samples were different and always above the background level in the Earth's crust (Figure 11 Left). Furthermore, Sr, Rb, W, K, Th, and Zr can take the form of natural mineral concentrations of zircon [59,60].

5.2. Characteristics of the Distributions of Identified Clusters

The samples from Cluster 1 were primarily characterized by the pronounced presence of calcium and strontium, as well as the highest median concentrations of iron, manganese, zinc, nickel, and barium. Cluster 2 featured elevated concentrations of potassium, rubidium, chromium, titanium, and zirconium. Cluster 3 included most of the samples whose concentrations were below the limits of detection of lead, nickel, vanadium, and manganese. This cluster was generally characterized by the lowest concentrations of the analyzed elements (both median and minimum values).

Based on the results, Figure 12 shows the spatial distribution of the samples in the identified clusters.
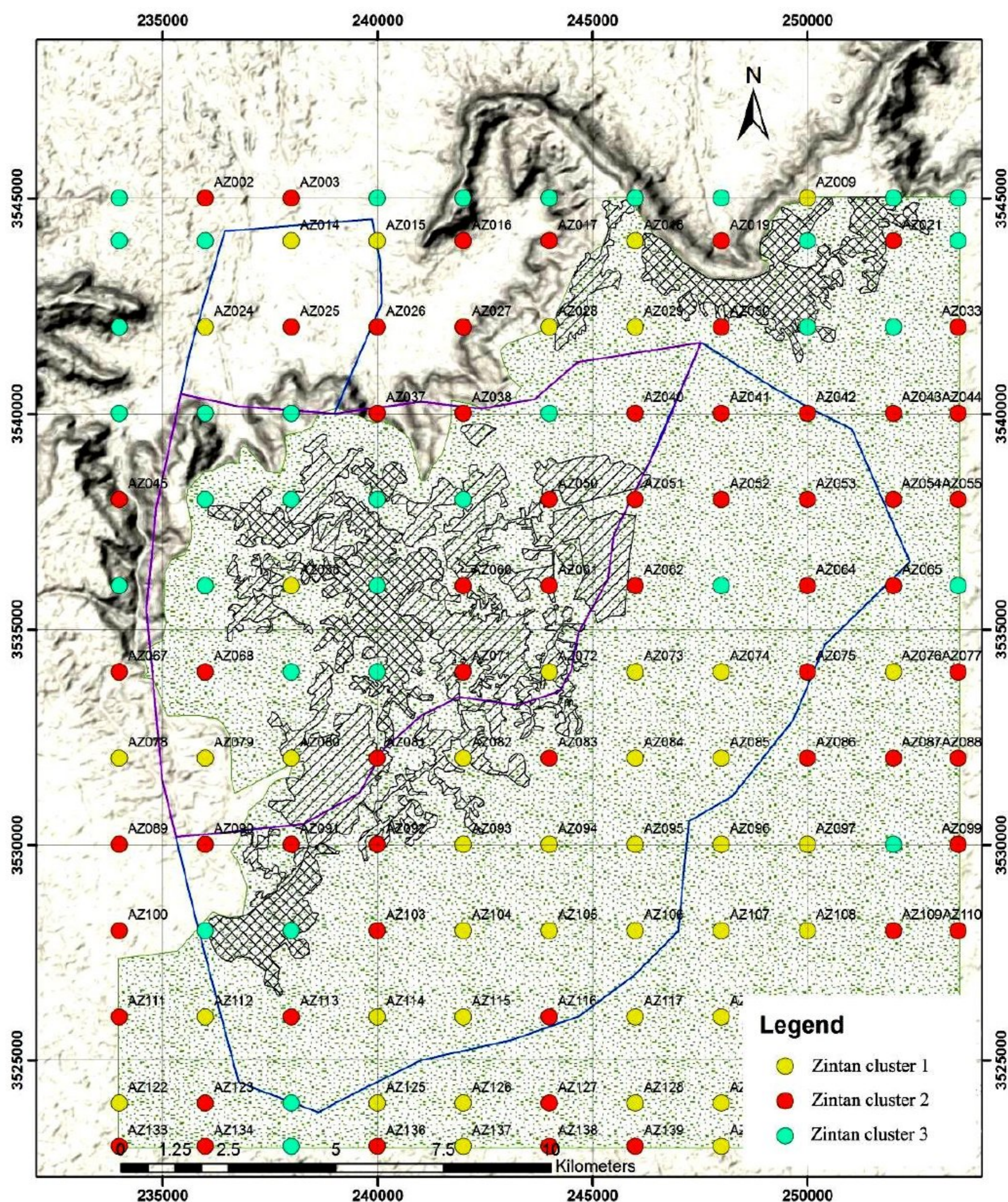
Figure 12. Spatial distribution of Cluster 1 (yellow dots), Cluster 2 (red dots), and Cluster 3 (green dots) samples. Raster-based SAS Planet Landscape w/o names (Google). The violet line on the map is the boundary of the old city of Zintan, and the external polygon (blue and violet lines) is the boundary of Zintan. The densely hatched polygons are the more densely populated areas; the less-hatched polygons are the less-populated areas, and the area with small green dots is agricultural, mostly sandy soil.

Cluster 1 generally contains samples collected in agricultural areas (Figure 12, yellow dots), Cluster 2 features samples from areas of intensive farming (Figure 12, red dots), and Cluster 3 largely includes samples associated with urban areas (Figure 12, green dots).

6. Conclusions

The surface layer of the soil within the city limits of Zintan was sampled to determine the distributions of PTEs. The study area was 19.5 × 22 km, and 143 samples were collected across a grid of roughly 2 × 2 km. Using an XRF analyzer (Thermo Fisher Scientific Niton XL3t GOLDD+), the samples were tested for the presence of the following elements: Mo, Zr, Sr, U, Rb, Th, Pb, Au, Se, As, Hg, Zn, W, Cu, Ni, Co, Fe, Mn, Cr, V, Ti, Sc, Ca, K, S, Ba, Cs, Te, Sb, Sn, Cd, Pd, and Ag. The modal analyses provided data on the natural mineral compositions of the samples. Minerals carry elements with natural impurities (accessory

elements) at times. This was taken into consideration, as a kind of benchmark for the detected elements of natural origin.

Three clusters were distinguished by a multivariate analysis of the results. They generally represented the following: less populated zones, within which the population engages in small-scale agricultural production (Cluster 1), a location where there is only agricultural production (Cluster 2), which can be classified as an area of intensive farming, and, in particular, an urban environment (Cluster 3).

Certain elements were found in all or in over 80% of the samples (Cr, Ni, V, Ti, Mn, Fe, Ba, Ca, Sr, Rb, K, and Zr) and they were most likely the result of natural features, i.e., the geological characteristics of the wider environment of the study area. The zones where the remaining elements were found in a small number of samples were most likely due to anthropogenic factors.

In addition to the above elements, which were a result of the geological setting (i.e., of natural origin), elements were detected in a small number of samples, probably of anthropogenic origin.

Finally, it can be stated that at the time of this research (the end of 2017), there was no excessive risk of pollution in the extended area of Zintan. The concentrations of elements of natural origin generally did not exceed the maximum permissible levels, while the elevated concentrations of elements of anthropogenic origin were mainly the result of agricultural activity, given that the most contaminated zones were on the northwestern plain and in agricultural areas. It is interesting to note that markedly elevated concentrations of pollutants were rarely detected in either densely or sparsely populated areas. All locations where concentrations of potentially toxic elements were determined to be higher than maximum permissible concentrations should be examined in detail.

Author Contributions: conceptualization, B.V. and V.R.V.; methodology, B.V., Z.N. and S.B.; resources, T.Đ., V.G. and S.B.; writing—original draft preparation, B.V., V.R.V., Z.N. and J.Š.; writing—review and editing, B.V., V.R.V. and Z.N.; statistical data processing, J.Š.; visualization, T.Đ. and V.G.; project administration, V.R.V.; field work and sampling, T.M.A. All authors have read and agreed to the published version of the manuscript.

Data Availability Statement: The data presented in this study are available on request from the corresponding authors.

Conflicts of Interest: The authors declare no conflict of interest.

References

1. Yan, X.; Liu, M.; Zhong, J.; Guo, J.; Wu, W. How Human Activities Affect Heavy Metal Contamination of Soil and Sediment in a Long-Term Reclaimed Area of the Liaohe River Delta, North China. *Sustainability* **2018**, *10*, 338. [CrossRef]
2. Imperato, M.; Adamo, P.; Naimo, D.; Arienzo, M.; Stanzione, D.; Violante, P. Spatial distribution of heavy metals in urban soils of Naples city (Italy). *Environ. Pollut.* **2003**, *124*, 247–256. [CrossRef] [PubMed]
3. Li, J.G.; Pu, L.J.; Liao, Q.L.; Zhu, M.; Dai, X.Q.; Xu, Y.; Zhang, L.F.; Hua, M.; Jin, Y. How anthropogenic activities affect soil heavy metal concentration on a broad scale: A geochemistry survey in Yangtze River Delta, Eastern China. *Environ. Earth Sci.* **2015**, *73*, 1823–1835. [CrossRef]
4. Banat, K.M.; Howari, F.M.; Al-Hamad, A.A. Heavy metals in urban soils of central Jordan: Should we worry about their environmental risks? *Environ. Res.* **2005**, *97*, 258–273. [CrossRef]
5. Yaylalı-Abanuz, G. Heavy metal contamination of surface soil around Gebze industrial area, Turkey. *Microchem. J.* **2011**, *99*, 82–92. [CrossRef]
6. Gehendra, K. *Impacts of Urbanization on Environmental Resources: Land Use Planning Perspective, Master of City and Regional Planning*; The University of Texas at Arlington: Arlington, TX, USA, 2010; pp. 1–58. Available online: https://rc.library.uta.edu/uta-ir/bitstream/handle/10106/5477/Kharel_uta_2502M_10978.pdf;sequence=1 (accessed on 25 April 2023).
7. Mohit, S.R. Impact of urbanization on Environmental. *Int. J. Emerg. Technol.* **2017**, *8*, 127–129.
8. Sheykhi, M.T. Mutual Effects of Environment and Urbanization: A Sociological Assessment. *Ann. Environ. Sci. Toxicol.* **2020**, *4*, 24–26. [CrossRef]

9. Ruiz Rincon, V.; Martinez-Alier, J.; Mingorria, S. Environmental Conflicts Related to Urban Expansion Involving Agrarian Communities in Central Mexico. *Sustainability* **2019**, *11*, 6545. [CrossRef]
10. Arndt, N.T.; Fontbote, L.; Hedenquist, J.W.; Kesler, S.E.; Thompson, J.F.H.; Wood, D. Future global mineral resources. *Geochem. Perspect.* **2017**, *6*, 1–171. [CrossRef]
11. Tompson, J.; Eagle, L.; Bonham, O. Resources for future generations—Understanding earth and people. *Eur. Geol. J.* **2017**, *44*, 11–15.
12. Silva, H.F.; Silva, N.F.; Oliveira, C.M.; Matos, M.J. Risk Assessment of Soil Contamination with Heavy Metals from Municipal Sewage Sludge. *Appl. Sci.* **2021**, *11*, 548. [CrossRef]
13. Pouyat, R.V.; Trammell, T.L.E. Chapter 10—Climate change and urban forest soils. *Dev. Soil Sci.* **2019**, *36*, 189–211.
14. Gao, Z.; Dong, H.; Wang, S.; Zhang, Y.; Zhang, H.; Jiang, B.; Liu, Y. Geochemical Characteristics and Ecological Risk Assessment of Heavy Metals in Surface Soil of Gaomi City. *Int. J. Environ. Res. Public Health* **2021**, *18*, 8329. [CrossRef]
15. Yadav, I.C.; Devi, N.L.; Singh, V.K.; Li, J.; Zhang, G. Spatial distribution, source analysis and health risk assessment of heavy metals contamination in house dust and surface soil from four major cities of Nepal. *Chemosphere* **2019**, *218*, 1100–1113. [CrossRef]
16. Silva, H.F.; Silva, N.F.; Oliveira, C.M.; Matos, M.J. Heavy Metals Contamination of Urban Soils—A Decade Study in the City of Lisbon, Portugal. *Soil Syst.* **2021**, *5*, 27. [CrossRef]
17. Mehmood, S.; Wang, X.; Ahmet, W.; Imtiaz, M.; Ditta, A.; Rizwan, M.; Irshad, S.; Basir, S.; Saeed, Q.; Mustafa, A.; et al. Removal Mechanisms of slag against potentially toxic elements in soil and plants for sustainable agricultural development: A critical review. *Sustainability* **2021**, *13*, 5255. [CrossRef]
18. Chibuike, G.U.; Obiora, S.C. Heavy Metal Polluted Soils: Effect on Plants and Bioremediation Methods. *Appl. Environ. Soil Sci.* **2014**, *2014*, 752708. [CrossRef]
19. Borozan, A.B.; Misca, C.D.; Morar, A.; Obistioiu, D.; Raba, D.N.; Pirvulescu, L.; Caba, I.L.; Alexa, E.; Poiana, M.; Bordean, D.; et al. Soil pollution with heavy metals and bioremediation methods. *AgroLife Sci. J.* **2021**, *10*, 54–66. [CrossRef]
20. Alinia-Ahandani, E.; Alizadeh-Terepoei, Z.; Sheydaei, M.; Peysepar-Balalami, F. Assessment of Soil on Some Heavy Metals and its Pollution in Roodsar-Iran. *Bimedical J. Sci. Tech. Res.* **2020**, *28*, 21977–21979. [CrossRef]
21. Zhou, H.; Yang, W.T.; Zhou, X.; Liu, L.; Gu, J.F.; Wang, W.L.; Zou, J.L.; Tian, T.; Peng, P.Q.; Liao, B.H. Accumulation of heavy metals in vegetable species planted in contaminated soils and the health risk assessment. *Int. J. Environ. Res. Public Health* **2016**, *13*, 289. [CrossRef]
22. Tóth, G.; Hermann, T.; Da Silva, M.R.; Montanarella, L. Heavy metals in agricultural soils of the European Union with implications for food safety. *Environ. Int.* **2016**, *88*, 299–309. [CrossRef]
23. Bystricka, J.; Kavalcova, P.; Musilova, J.; Karovicova, J.; Kuchtova, V. The effect of variety on heavy metals intake by onion grown in contaminated soil. In Proceedings of the 14th International Conference on Environmental Science and Technology Greece, Rhodes, Greece, 3–5 September 2015.
24. Hatem, M.; Parvez, I.H.; Eid, I.B. Estimated dietary intakes of toxic elements from four staple foods in Najran city, Saudi Arabia. *Int. J. Environ. Res. Public Health* **2017**, *14*, 1575.
25. Saint-Laurent, D.; Hähni, M.; St-Laurent, J.; Baril, B. Comparative Assessment of Soil Contamination by Lead and Heavy Metals in Riparian and Agricultural Areas (Southern Québec, Canada). *Int. J. Environ. Res. Public Health* **2010**, *7*, 3100–3114. [CrossRef]
26. Santos-Francés, F.; Martínez-Graña, A.; Ávila Zarza, C.; García Sánchez, A.; Alonso Rojo, P. Spatial distribution of heavy metals and the environmental quality of soil in the Northern Plateau of Spain by geostatistical methods. *Int. J. Environ. Res. Public Health* **2017**, *14*, 568. [CrossRef] [PubMed]
27. Bortey-Sam, N.; Nakayama, S.M.M.; Akoto, O.; Ikenaka, Y.; Baidoo, E.; Mizukawa, H.; Ishizuka, M. Ecological risk of heavy metals and a metalloid in agricultural soils in Tarkwa, Ghana. *Int. J. Environ. Res. Public Health* **2015**, *12*, 11448–11465. [CrossRef]
28. Song, D.; Zhuang, D.; Jiang, D.; Fu, J.; Wang, Q. Integrated health risk assessment of heavy metals in Suxian County, South China. *Int. J. Environ. Res. Public Health* **2015**, *12*, 7100–7117. [CrossRef] [PubMed]
29. Zurqani, H.A.; Mikhailova, E.A.; Post, C.J.; Schlautman, M.A.; Elhawej, A.R. A Review of Libyan Soil Databases for Use within an Ecosystem Services Framework. *Land* **2019**, *8*, 82. [CrossRef]
30. Chandini, R.K.; Kumar, R.; Om, P. The impact of Chemical Fertilizers on our Environment and Ecosystem. In *Research Trends in Environmental Sciences*, 2nd ed.; AkiNik Publications: Delhi, India, 2020.
31. Rahimi, A.; Moghaddam, S.S.; Ghiyasi, M.; Heydarzadeh, S.; Ghazizadeh, K.; Popović-Djordjević, J. The Influence of Chemical, Organic and Biological Fertilizers on Aerobiological and Antioxidant Properties of Syrian Cephalaria (*Sephalaria syriaca* L.). *Agriculture* **2019**, *9*, 122. [CrossRef]
32. Viets, F.G.; Lunin, J. The environmental impact of fertilizers. *CRC Crit. Rev. Environ. Control* **1975**, *5*, 423–453. [CrossRef]
33. Ning, C.C.; Gao, P.D.; Wang, B.Q.; Lin, W.P.; Jiang, N.H.; Cai, K.Z. Impacts of chemical fertilizer reduction and organic amendments supplementation on soil nutrient, enzyme activity and heavy metal content. *J. Integr. Agric.* **2017**, *16*, 1819–1831. [CrossRef]
34. Available online: http://weekly.ahram.org.eg/News/6476.aspx (accessed on 23 July 2023).
35. Asketell, J.M.; Ghellali, S.M. A palaeogeologic map of the pre-Tertiary surface in the region of the Jifarah Plain: Its implication to the structural history of Northern Libya. In *The Geology of Libya. Volume IV–VII: Third Symposium on the Geology of Libya, Held at Tripoli, 27–30 September 1987*; Salime, M.J., Ed.; Elsevier: Amsterdam, The Netherlands, 1991; Volume 6, pp. 2381–2406.
36. Antonović, A. *Geological Map of Libya 1:250000, Sheet Mizdah, NH 33-1, Socialist People's Libyan Arab Jamahitiyah*; Industrial Research Centre Tripoli: Tajoura, Libia, 1977.

37. Briffa, J.; Sinarga, E.; Blundell, R. Heavy metal pollution in the environment and their toxicological effects on humans. *Heliyon* **2020**, *6*, e04691. [CrossRef]

38. Mitra, S.; Chakraborty, A.J.; Tareq, A.M.; Emran, T.B.; Nainu, F.; Khusro, A.; Idris, A.M.; Khandaker, M.U.; Osman, H.; Alhumaydhi, F.A.; et al. Imapct of heavy metals on the environment and human health: Novel therapeutic insights to counter of toxicity. *J. King Saud Univ. Sci.* **2022**, *34*, 101865. [CrossRef]

39. Available online: https://en.db-city.com/Libyan-Arab-Jamahiriya{-}{-}Jabal-al-Gharbi{-}{-}Zintan (accessed on 3 August 2023).

40. Available online: https://libyaobserver.ly/culture/city-zintan (accessed on 3 August 2023).

41. Güler, C.; Thyne, G.D.; Mccray, J.E. Evaluation of Graphical and Multivariate Statistical Methods for Classification of Water Chemistry Data. *Hydrogeol. J.* **2002**, *10*, 455–474. [CrossRef]

42. Cloutier, V.; Lefebvre, R.; Therrien, R.; Savard, M.M. Multivariate statistical analysis of geochemical data as indicative of the hydrogeochemical evolution of groundwater in a sedimentary rock aquifer system. *J. Hydrol.* **2008**, *353*, 294–313. [CrossRef]

43. Helena, B.A.; Vega, M.; Barrado, E.; Pardo, R. A Case of Hydrochemical Characterization of an Alluvial Aquifer Influenced by Human Activities. *Water Air Soil Pollut.* **1999**, *112*, 365–387. [CrossRef]

44. Micó, C.; Recatalá, L.; Peris, M.; Sánchez, J. Assessing heavy metal sources in agricultural soils of a European Mediterranean area by multivariate analysis. *Chemosphere* **2006**, *65*, 863–872. [CrossRef]

45. LST Heavy Liquid Background and Properties. Available online: https://heavyliquids.com (accessed on 3 August 2023).

46. Mirković, M. Izveštaj o Sedimentološkim Ispitivanjima Stena, Kvantitativna i Kvalitativna Analiza Sadržaja Minerala Teške i Lake Frakcije; Geološki Zavod Srbije: Beograd, Srbija, 2018; pp. 1–5.

47. Available online: http://www.epa.state.il.us/land/ccdd/new-max-allowable-concentrations-table.pdf (accessed on 20 November 2022).

48. Vodyanitskii, Y.N. Standards for the contents of heavy metals in soil of some states. *Ann. Agrar. Sci.* **2016**, *14*, 257–263. [CrossRef]

49. Available online: https://www.pravno-informacioni-sistem.rs/SlGlasnikPortal/eli/rep/sgrs/vlada/uredba/2010/88/2/reg (accessed on 20 November 2022).

50. Available online: https://en.wikipedia.org/wiki/Abundance_of_the_chemical_elements (accessed on 20 November 2022).

51. Available online: http://www.daviddarling.info/encyclopedia/E/elterr.html (accessed on 20 November 2022).

52. Nunes, N.; Ragonezi, C.; Gouveia, C.; Pinheiro, C.; Miguel, Â. Review of Sewage Sludge as a Soil Amendment in Relation to Current International Guidelines: A Heavy Metal Perspective. *Sustainability* **2021**, *13*, 2317. [CrossRef]

53. Li, Y.; Ye, F.; Wang, A.; Wang, D.; Yang, B.; Zheng, Q.; Sun, G.; Gao, X. Chronic Arsenic Poisoning Probably Caused by Arsenic-Based Pesticides: Findings from an Investigation Study of a Household. *Int. J. Environ. Res. Public Health.* **2016**, *16*, 133. [CrossRef]

54. Blaschko, S.D.; Chi, T.; Miller, J.; Flechner, L.; Fakra, S.; Kapahi, P.; Kahn, A.; Stoller, M.L. Strontium substitution for calcium in lithogenesis. *J. Urol.* **2013**, *189*, 735–739. [CrossRef]

55. Available online: https://www.oilandgasonline.com/doc/cesium-formate-fluids-0001 (accessed on 21 November 2022).

56. Hart, S.R. K, Rb, Cs contents and K/Rb, K/Cs ratios of fresh and altered submarine basalts. *Earth Planet. Sci. Lett.* **1969**, *6*, 295–303. [CrossRef]

57. Griffin, W.L.; Murthy, V.R. Abundances of K, Rb, Sr and Ba in some ultramafic rocks and minerals. *Earth Planet. Sci. Lett.* **1968**, *4*, 497–501. [CrossRef]

58. Available online: https://www.bighaat.com/products/multiplex-molybdenum (accessed on 21 November 2022).

59. Belousova, E.A.; Griffin, W.L.; O'Reilly, S.Y.; Fisher, N.I. Igneous zircon: Trace element composition as an indicator of source rock type. *Contrib. Mineral. Petrol.* **2002**, *143*, 602–622. [CrossRef]

60. Yang, W.; Zhang, M.; Yan, J.; Chen, X. Zircon U-Pb Ages and Geochemistry of the Granite in the Xintianling Tungsten Deposit, SE China: Implications for Geodynamic Settings of the Regional Tungsten Mineralization. *Minerals* **2022**, *12*, 952. [CrossRef]